A Search for Gamma-Ray Prompt Emission Associated with the Lorimer Burst FRB 010724

C. Guidorzi[1] , M. Marongiu[1,2] , R. Martone[1,2] , L. Amati[3] , F. Frontera[1,3] , L. Nicastro[3] , M. Orlandini[3] ,
R. Margutti[4] , and E. Virgilli[1]

[1] Department of Physics and Earth Science, University of Ferrara, via Saragat 1, I-44122, Ferrara, Italy
[2] ICRANet, Piazza della Repubblica 10, I-65122 Pescara, Italy
[3] INAF—Osservatorio di Astrofisica e Scienza dello Spazio di Bologna, Via Piero Gobetti 93/3, I-40129 Bologna, Italy
[4] Center for Interdisciplinary Exploration and Research in Astrophysics and Department of Physics and Astronomy, Northwestern University, 2145 Sheridan Road, Evanston, IL 60208-3112, USA

Abstract

No transient electromagnetic emission has yet been found in association to fast radio bursts (FRBs), the only possible exception (3σ confidence) being the putative γ-ray signal detected in *Swift*/Burst Alert Telescope data in the energy band 15–150 keV at the time and position of FRB 131104. Systematic searches for hard X/γ-ray counterparts to other FRBs ended up with just lower limits on the radio/γ-ray fluence ratios. In 2001, at the time of the earliest discovered FRBs, the *BeppoSAX* Gamma-Ray Burst Monitor (GRBM) was one of the most sensitive open-sky γ-ray monitors in the 40–700 keV energy band. During its lifetime, one of the FRBs with the highest radio fluence ever recorded, FRB 010724 (800 ± 400 Jy ms), also known as the "Lorimer burst," was promptly visible to the GRBM. Upon an accurate modeling of the GRBM background, eased by its equatorial orbit, we searched for a possible γ-ray signal in the first 400 s following the FRB, similar to that claimed for FRB 131104 and found no significant emission down to a 5σ limit in the range $(0.24–4.7) \times 10^{-6}$ erg cm^{-2} (corresponding to 1 and 400 s integration time, respectively), in the energy band 40–700 keV. This corresponds to $\eta = F_{\mathrm{radio}}/F_{\gamma > 10^{8-9}}$ Jy ms erg^{-1} cm^2, i.e., the deepest limit on the ratio between radio and γ-ray fluence, which rules out a γ-ray counterpart similar to that of FRB 131104. We discuss the implications on the possible mechanisms and progenitors that have been proposed in the literature, also taking into account its relatively low dispersion measure (375 ± 3 pc cm^{-3}) and an inferred redshift limit of $z < 0.4$.

Key words: radiation mechanisms: non-thermal – stars: individual (FRB 010724)

1. Introduction

Fast radio bursts (FRBs) are ms-long bright pulses of unknown origin characterized by a dispersion measure (DM) significantly in excess of the corresponding Galactic value (Lorimer et al. 2007; Thornton et al. 2013). A large DM value, due to a relatively large electron column density integrated along the sightline, strongly hints at an extragalactic origin. Despite the high all-sky daily rate of several thousands (e.g., Crawford et al. 2016; Rane et al. 2016; Scholz et al. 2016), only ∼80 FRBs have been publicly announced so far (as of 2019 July; Petroff et al. 2016). This is mainly due to the relatively narrow fields of view (FOV) of most of the radiotelescopes that first observed them, although the discovery rate is now ramping up thanks to a new generation of wide FOV experiments that have recently come on stage. The majority of them appear to be one-off events, except for a couple of them (Spitler et al. 2016; CHIME/FRB Collaboration et al. 2019). See Petroff et al. (2019a), Katz (2018), Popov et al. (2018), and Rane & Lorimer (2017) for updated reviews.

Affected by several arcmin positional uncertainty, FRBs so far defied any search for either prompt simultaneous or afterglow transient emission at other wavelengths that would help identify their host galaxies, measure the distance, constrain the radiation mechanism and the nature of the progenitor. There are a few exceptions. FRB 121102, whose host was found at a redshift of $z = 0.193$ (Tendulkar et al. 2017), which is also one of the two repeating sources; it was precisely its repeating nature that made it possible to localize with sub-arcsec accuracy during interferometric radio

observations (Chatterjee et al. 2017). Recently, the redshifts of two other non-repeating FRBs have been determined: FRB 180924 at $z = 0.3214$ (Bannister et al. 2019) and FRB 190523 at $z = 0.66$ (Ravi et al. 2019).

A possible (3σ confidence) γ-ray ∼400 s long transient source, Swift J0644.5-5111, positionally and temporally compatible with FRB 131104, was reported by DeLaunay et al. (2016, hereafter D16) in the 15–150 keV band within the data of the Burst Alert Telescope (BAT; Barthelmy et al. 2005) aboard the *Neil Gehrels Swift Observatory* (Gehrels et al. 2004). The possibility of a gamma-ray burst (GRB) associated to this FRB was later called into question by the lack of any radio afterglow (Shannon & Ravi 2017). However, admitting microphysical shock parameter values different from what is typically assumed for GRB afterglows, this GRB–FRB association remains plausible (Gao & Zhang 2017). A similar search carried out by D16 for other FRBs that were promptly visible with BAT yielded only upper limits. Previous searches for high-energy counterparts to FRBs had ended up with lower limits to the radio/γ fluence ratio $\eta_{\mathrm{frb}} > 10^{7-9}$ Jy ms erg^{-1} cm^2, incompatible with the upper limit $\eta_{\mathrm{sgr}} < 10^{7}$ Jy ms erg^{-1} cm^2 derived for the γ-ray giant flare of the Galactic magnetar SGR 1806-20 (Tendulkar et al. 2016). Similarly, Scholz et al. (2017) analyzed the data of the Gamma-Ray Burst Monitor (GRBM; Meegan et al. 2009) aboard the *Fermi Gamma-ray Telescope* and found nothing down to 10^{-8} erg cm^{-2} in the 10–100 keV energy band in a 2 s window centered on the arrival times of four bursts of repeater FRB 121102. Reversing the approach, Palaniswamy et al. (2014) found no prompt radio

Table 1
BeppoSAX/GRBM Data Availability for the FRBs Detected in 2001

FRB	UT	R.A.(J2000) (deg)	Decl.(J2000) (deg)	ϕ (deg)	θ (deg)	Elevation (deg)	OP	Comment
010125	00:29:14	286.7	−40.7	42.2	19.4	−18.0	10600	Earth-blocked
010312[a]	11:06:48	81.7	−64.9	⋯	⋯	1.4	10862	no data
010621	13:02:09	283.0	−8.5	203.5	−8.8	59.5	11411	unavailable due to data gap
010724	19:50:00	19.5	−75.2	162.0	−43.5	38.6	11651	visible and available

Notes. (ϕ, θ) is the direction with respect to the *BeppoSAX* payload reference frame (Frontera et al. 2009). The elevation angle is calculated with respect to the Earth limb. OP is the observing period, which identifies the data set in the *BeppoSAX* archive.
[a] Reported by Zhang et al. (2019).

pulses compatible with FRBs associated to five GRBs that were observed starting within 140 s of the γ-ray trigger time. No detections were reported from searches in the GeV domain using the *Fermi* Large Area Telescope (Atwood et al. 2009) for both one-off FRBs (Yamasaki et al. 2016; Xi et al. 2017) and repeaters (Zhang & Zhang 2017; Yang et al. 2019). Analogous results were obtained at very high energies, above 100 GeV (H.E.S.S. Collaboration et al. 2017; MAGIC Collaboration et al. 2018) as well as for TeV–PeV neutrinos coincident with FRBs (Aartsen et al. 2018; Albert et al. 2019).

One of the open questions is whether a common family of progenitors is responsible for the observed population of FRBs, in particular one-off and repeating sources (Palaniswamy et al. 2018; Caleb et al. 2019), or, as in the case of GRBs, at least two families are required to explain the long and short duration events respectively associated to the core collapse of some kind of hydrogen-stripped massive stars and to the merging of compact objects (see Kumar & Zhang 2015 for a review). Thus, the existence of repeating sources does not necessarily rule out the so-called cataclysmic models. A number of the proposed models that predict an associated high-energy emission invoke rapidly rotating young neutron stars (NS) and magnetars as progenitors (Katz 2014; Cordes & Wasserman 2016; Lyutikov et al. 2016). Given also that in some models ms magnetars are supposed to form following the core collapse that powers both long (Usov 1992; Thompson 1994; Bucciantini et al. 2007; Metzger et al. 2011) and short GRBs (Fan & Xu 2006; Metzger et al. 2008; Rowlinson et al. 2010; Gompertz et al. 2013), as well as superluminous supernovae (SLSNe; Murase et al. 2016; Metzger et al. 2017; Nicholl et al. 2017), it is worth searching for hard X/γ-ray emission associated to FRBs. As with GRBs and SNe the study of the environments may potentially provide useful clues on the homogeneity of the FRB progenitors (Eftekhari & Berger 2017).

Motivated by the results of D16, we exploited the sensitivity of the GRBM (Frontera et al. 1997) that operated as an open-sky detector in the energy band 40–700 keV aboard *BeppoSAX* (Boella et al. 1997) in 1996–2002. We carried out a detailed search for a high-energy counterpart to FRB 010724, the first reported FRB (Lorimer et al. 2007), popularly known as the Lorimer burst: this was so bright that it saturated the Parkes multibeam receiver and was also detected in three other beams of the receiver. From an initial estimate of 150 Jy ms, its fluence has recently been revised to 800 ± 400 Jy ms (Ravi 2019). Owing to its exceptional brightness, FRB 010724 might represent a discovery bias (Macquart & Ekers 2018) and may come from a space-limited population, whose local density would far exceed the cosmological one (Katz 2016). Given its relatively low DM of 375 ± 3 pc cm^{-3}, evidence that this FRB might be relatively

nearby is also provided by the brightness-dispersion correlation shown in the Australian Square Kilometre Array Pathfinder sample (Shannon et al. 2018; see also Niino 2018). In this respect, another example of low-DM/high-flux FRB is given by FRB 110214 (Petroff et al. 2019b). We therefore discuss the implications of our results on the proposed associations as a function of the possible redshift compatibly with its DM. Hereafter, we assume the latest Planck cosmological parameters: $H_0 = 67.74$ km s^{-1} Mpc^{-1}, $\Omega_m = 0.31$, $\Omega_\Lambda = 0.69$ (Planck Collaboration et al. 2016).

2. Data Analysis

From the FRB catalog[5] (Petroff et al. 2016) we selected the four FRBs that occurred in 2001 during the *BeppoSAX* operational life (Table 1) and checked the availability of GRBM data at the time of each FRB along with its visibility (i.e., not Earth-blocked). Only FRB 010724 passed the selection.

Based on the direction of FRB 010724 with reference to the *BeppoSAX* frame, the expected signal for each of the four GRBM units is comparable with each another (Table 2). From the *BeppoSAX* GRB catalog (Frontera et al. 2009) we used the response matrices of the GRB with the nearest local position $(158°, -46°)$ to that of the FRB $(162°, -43°.5)$, and for each unit we calculated the expected number of counts for both energy bands 40–700 keV and >100 keV, assuming the same spectral models and γ-ray fluences found by D16 for FRB 131104 (Table 2). No prompt *BeppoSAX* X-ray data are available for FRB 010724, because it lies outside the FOV of the Wide Field Cameras (Jager et al. 1997).

We modeled the background rates for each unit and energy band by exploiting the GRBM data sharing the most similar configuration and that were acquired about one day before the FRB. A detailed description is reported in the Appendix.

3. Results

In order to investigate a potential γ-ray counterpart, we assumed a fast-rise, slow-decay pulse profile as modeled by Kocevski et al. (2003) so as to have the desired duration of ∼400 s. We chose the following parameters: rise and decay indices $r = 2$ and $d = 3$, respectively; peak time $t_m = 100$ s and $t_0 = 0$. Normalizations were chosen so as to match the expected counts (Section 2) in the time interval from 0 to 400 s, comparable with the $T_{90} = 377$ s of the *Swift* event. The resulting profiles are shown in Figure 1 with dashed lines, added to the background level, for the 40–700 keV channels of each of the detectors, as

_____
5 http://www.frbcat.org

Table 2
Expected Net Counts for a γ-Ray Event Equal to that Found for FRB 131104[a]

Model[b]	Γ	kT (keV)	$F_\gamma(40–700)$ (erg cm^{-2})	Band (keV)	GRBM1 (counts)	GRBM2 (counts)	GRBM3 (counts)	GRBM4 (counts)	Mean (counts)	5σ U.L. on F_γ[c] (erg cm^{-2})
POW	1.16[d]	⋯	1.5×10^{-5}	40–700	4698	3573	4916	7248	5109	$<4.0 \times 10^{-6}$
		⋯		>100	4286	3129	4381	7032	4707	
POW	0.38[d]	⋯	4.9×10^{-5}	40–700	16754	11971	17188	25820	17933	$<3.7 \times 10^{-6}$
		⋯		>100	16303	11370	16722	26938	17833	
POW	1.84[d]	⋯	6.1×10^{-6}	40–700	1603	1316	1696	2392	1752	$<4.7 \times 10^{-6}$
		⋯		>100	1304	1024	1338	2122	1447	
POW	2	⋯	5.0×10^{-6}	40–700	1259	1055	1332	1852	1374	$<5.0 \times 10^{-6}$
		⋯		>100	991	793	1012	1600	1099	
TB	⋯	200	4.2×10^{-6}	40–700	1017	896	1097	1472	1120	$<4.7 \times 10^{-6}$
	⋯			>100	741	628	760	1182	828	
TB	⋯	75	2.3×10^{-6}	40–700	410	405	439	522	444	$<7.1 \times 10^{-6}$
	⋯			>100	227	218	219	325	247	

Notes.
[a] Counts are meant to be in excess of the background for each GRBM unit for a γ-ray event with $F_\gamma(15–150 \text{ keV}) = 4 \times 10^{-6}$ erg cm^{-2}.
[b] The spectral models are the same as in D16: power law (POW) and thermal bremsstrahlung (TB).
[c] Upper limits obtained by integrating the background-subtracted mean counts over the [0, 400] s interval.
[d] Photon index values corresponding to the confidence interval estimated by D16.
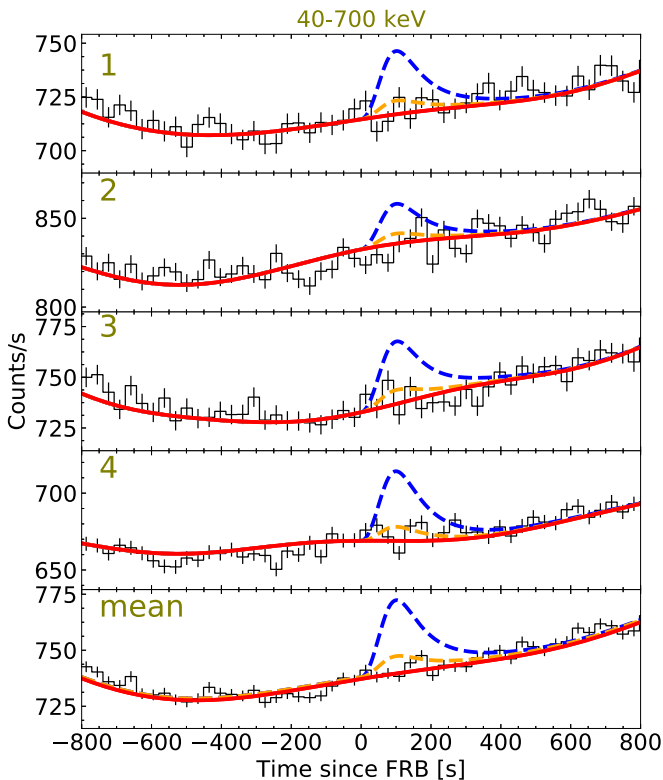

Figure 1. *BeppoSAX*/GRBM ratemeters (40–700 keV; bin time of 32 s) at the time of FRB 010724. Background (solid lines) was obtained modeling a different orbit. From top to bottom: individual units 1–4, the mean of the four units. Dashed blue (orange) profile is what one would expect for an event equal to that found by D16 in *Swift*/BAT data for FRB 131104 extrapolating the best-fit power-law (thermal bremsstrahlung) model to the 40–700 keV band.

well as for the average of the four, which has the best signal-to-noise ratio. Specifically, blue and orange lines correspond to the best-fit power law (hereafter POW) and thermal bremsstrahlung (hereafter TB) models, respectively. Furthermore, we integrated the background-subtracted counts in the 0–400 s time intervals and found no significant (>5σ) excess. The most constraining

upper limit to the 40–700 keV fluence is obtained from the mean time profile: a total count fluence of 247 ± 273 turns into a 5σ upper limit of $F_\gamma(40–700) < 4.7 \times 10^{-6}$ erg cm^{-2} for the POW and $F_\gamma(40–700) < 7.1 \times 10^{-6}$ erg cm^{-2} for the TB model, accounting for the uncertainties on the best-fit models. Assuming shorter γ-ray events and thus, integrating over shorter time intervals Δt, we found no >5σ excess, with the corresponding upper limits scaling approximately as $\sqrt{\Delta t}$. In particular, taking $\Delta t = 1$ s, i.e., the time bin of the FRB, limits scale down by a factor of ~19: $F_\gamma(40–700) < 2.5 \times 10^{-7}$ erg cm^{-2} and $<3.7 \times 10^{-7}$ erg cm^{-2} for the POW and TB models, respectively. Figure 2 shows the cumulative count fluence and corresponding values in physical units for a POW spectrum (using $\Gamma = 1.84$, which gives the most conservative limit on fluence) as a function of the integration time, along with the 5σ upper limit. The most significant excess in 40–700 keV is 3.3σ around $t = 14$ s. However, inspecting the individual detector profiles from Figure 1 suggests that it is mostly due to unit 3 and due to the background modeling inaccuracy rather than a genuine signal.

Consequently, a γ-ray counterpart equal to that of FRB 131104 cannot be ruled out for the TB model, whereas the POW model is rejected. Moreover, assuming a similar radio-γ spectral slope as the one found by D16, such a γ-ray counterpart is rejected with high confidence in the case of FRB 010724, given that the Lorimer burst has a radio fluence 340 ± 170 times as high as that of FRB 131104.

This γ-ray upper limit is the most constraining value for the radio-to-γ fluence ratio yet obtained for an FRB: $\log_{10}\eta > 8.2$ for POW and $\log_{10}\eta > 8.0$ for the TB model. These values are ~250 times higher than the value measured for FRB 131104, $\log_{10}\eta = 5.8 \pm 0.2$ (D16). Taking the limit derived for the 1 s bin centered on the FRB, the same limits on η become $\log_{10}\eta > 9.5$–9.3 for the POW and TB models, respectively. For reference, we also considered the case of a POW with $\Gamma = 2$ (Table 2): the most conservative upper limit changes only marginally.

As a further check, we exploited the 240-channel spectra continuously acquired by the GRBM units in the 40–700 keV energy band every 128 s (Frontera et al. 1997; Guidorzi et al. 2011) to investigate the possible presence of a signal in two
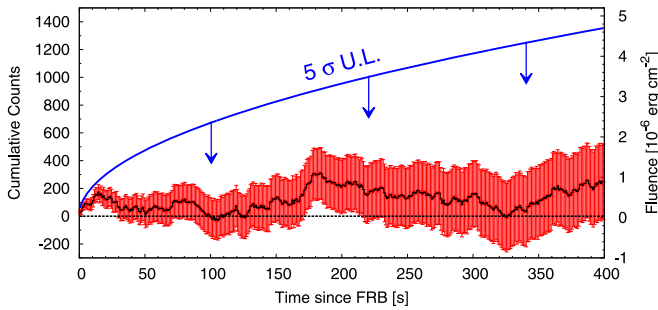
Figure 2. Cumulative net counts in the 40–700 keV energy band averaged over the four GRBM units as a function of integration time, from 0 to t, with t spanning the 0–400 s interval. Error bars are 1σ. The solid blue line shows the corresponding 5σ upper limits. The corresponding fluence (right-hand axis) is calculated assuming a power-law spectrum with $\Gamma = 1.84$.
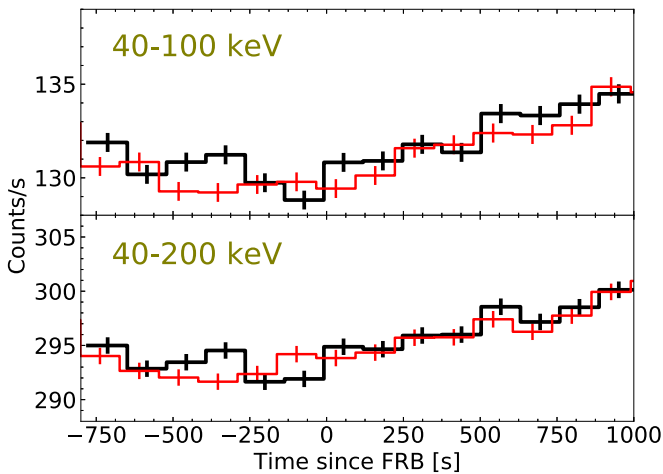

Figure 3. Mean count rates in two different energy bands with an integration time of 128 s, obtained from the 240-channel spectra continuously acquired by the GRBM units every 128 s. The FRB orbit rates (black) are shown together with the background orbit ones (red).

Figure 4. Top: emitted energy of the FRB (purple) and 5σ upper limits on the 400 s prolonged emission (lower boundary of the hatched region) and on the 1 s coincident with the FRB (dark blue). For comparison, also shown are the isotropic-equivalent energies of the extended emission often associated to short GRBs (yellow), which is roughly as energetic as the short GRB itself, the subluminous short GRB 170817A associated to the double NS merger GW170817 (green), magnetar giant flares (orange). Bottom: DM (red) due to the combination of the host galaxy (HG) and the local environment around the source (loc), estimated subtracting the IGM contribution from the excess DM, as a function of redshift. The maximum value of $z = 0.4$ corresponds to the case where all of the DM in excess of the Galactic value is due to the IGM. Also shown are the mean values of the expected DM due to the sightline within the host galaxy for two different kinds, dwarf and spiral galaxies, from simulations by Xu & Han (2015).

energy bands: 40–100 and 40–200 keV, respectively. Figure 3 displays the corresponding 128 s light curves averaged over the four units (black) along with the analogous data of the background orbit (red). Although the poorer temporal resolution does not allow us to model the background as accurately as we did for the 1 s ratemeters, yet the comparison between the FRB orbit and the background orbit rates excludes the possibility of a relatively soft signal associated with the FRB.

4. Discussion

We rule out a γ-ray transient event that is similar to Swift J0644.5-5111 for FRB 131104 (see D16). This is however assuming a POW spectrum; the softer case of a TB is only marginally excluded. A γ-ray signal, rescaled to the much higher radio fluence of the Lorimer burst, is also ruled out, regardless of the spectral mode. Therefore, if the association found by D16 is true, the Lorimer burst is intrinsically different and much more γ-ray quiet. Alternatively, the Lorimer burst was associated with an analogous γ-ray transient that was more collimated than the radio emission and that was not pointing toward Earth (e.g., Romero et al. 2016).

For FRB 010724 the DM excess, i.e., the measured DM removed from the Galactic contribution, is $DM_E = 330 \, pc \, cm^{-3}$
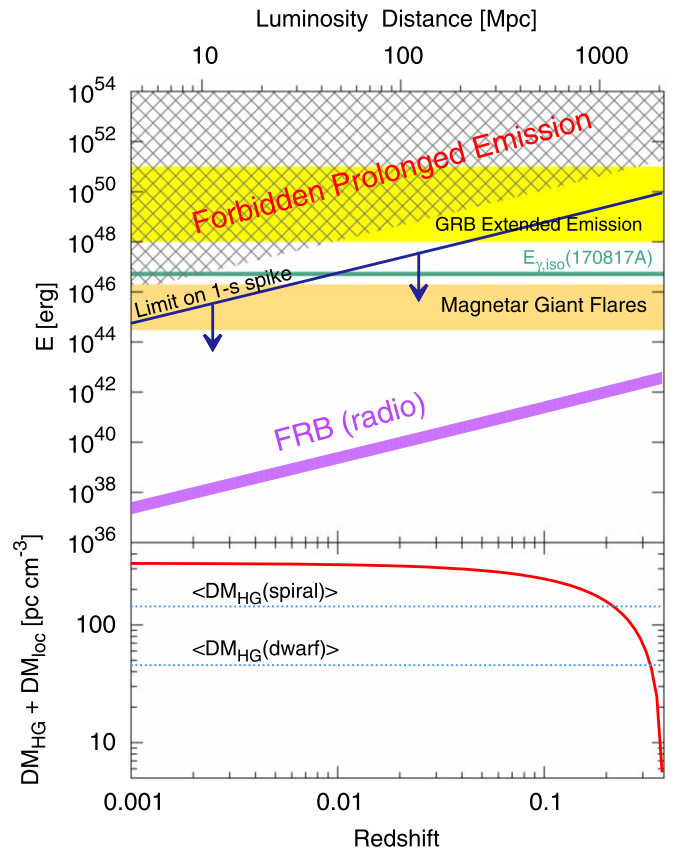
(Petroff et al. 2016) and can be expressed as the sum of different terms: the intergalactic medium (IGM), the host galaxy (HG), and the local environment surrounding the FRB source:

$$DM_E = DM_{IGM} + \frac{DM_{HG} + DM_{loc}}{1 + z}. \quad (1)$$

Using the relation by Zhang (2018) $z \sim D_{IGM}/(855 \, pc \, cm^{-3})$, an upper limit on redshift of $z < 0.4$ is obtained. Simulations suggest that the contribution of the host to the observed DM ranges from an average value of $45 \, pc \, cm^{-3}$ in the case of a dwarf galaxy all the way up to $\sim 142 \, pc \, cm^{-3}$ averaging over all inclination angles for a spiral (Xu & Han 2015).

Figure 4 summarizes our constraints for various models considered. Assuming that the host is a dwarf, similarly to long GRBs and SLSNe as is the case for the repeater FRB 121101 (Metzger et al. 2017; Tendulkar et al. 2017), and adopting for DM_{HG} the typical value expected for this kind of galaxies, the constraint on redshift becomes $z \lesssim 0.3$. Using the typical value for a spiral, i.e., about half of DM_E, the range shrinks to

$z \lesssim 0.2$. The same constraint holds assuming that half of DM_E is due to the local environment of the FRB progenitor. Making no assumption on DM_E, the energy of the radio pulse itself lies in the range $10^{38} < E_{radio}/erg < 6 \times 10^{42}$, in line with what has been argued for other FRBs, although at least 10 times more energetic than the individual bursts of the repeater FRB 121102 (Gourdji et al. 2019).

It is interesting to compare our limits on the γ-ray released energy with that of other astrophysical transients that have possible connections with FRBs. As shown in Figure 4, based on our analysis, we rule out the following interpretations:

1. a γ-ray spike due to an extragalactic magnetar giant flare with the same radio/γ-ray fluence ratio as that of the Galactic magnetar SGR 1806-20 (see also Tendulkar et al. 2016);
2. short GRBs with isotropic-equivalent energies $E_{\gamma,iso} > 10^{50}$ erg, that are the majority of the observed population (10^{49}–10^{52} erg; Fong et al. 2015);
3. the typical γ-ray emission of a cosmological long GRB, whose isotropic-equivalent energy ranges from $\sim 10^{51}$ up to $\sim 10^{55}$ erg (Tsvetkova et al. 2017).

On the other hand, we cannot reject the following scenarios:

1. an extragalactic giant flare as energetic as the few ones observed in our Galaxy (3×10^{44}–2×10^{46} erg; Mazets et al. 1979; Feroci et al. 2001; Hurley et al. 2005; Palmer et al. 2005; orange region in Figure 4), regardless of the radio/γ-ray spectral slope;
2. a relatively weak short GRB ($E_{\gamma,iso}$ in the range 10^{49}–10^{50} erg) at $z > 0.04$ ($D_L > 180$ Mpc);
3. a sub-energetic short GRB at $z > 0.01$ ($D_L > 45$ Mpc), such as GRB 170817A associated to GW170817, the first binary neutron star (BNS) merger detected with gravitational interferometers (Abbott et al. 2017a), which had $E_{\gamma,iso} = (5.3 \pm 1.0) \times 10^{46}$ erg. This holds true regardless of whether the GRB is truly sub-energetic or is a typical short GRB viewed off-axis, as was the case of GRB 170817A (Alexander et al. 2017, 2018; Granot et al. 2017; Margutti et al. 2017, 2018; Troja et al. 2017);
4. the presence of the so-called extended emission that characterizes some short GRBs. This is a faint, long-lasting ($\sim$few hundred seconds) hard X/γ-ray tail following the initial spike (Lazzati et al. 2001; Montanari et al. 2005; Norris & Bonnell 2006), whose isotropic-equivalent energy is in the range 10^{48}–10^{51} erg (Kisaka et al. 2017; Murase et al. 2017; yellow area in Figure 4);
5. the so-called low-luminosity (*ll*) long GRBs (Kulkarni et al. 1998; Campana et al. 2006; Waxman et al. 2007) having $E_{\gamma,iso} \sim 10^{48}$–$10^{50}$ erg. *ll*-GRBs probably represent a separate family (Amati et al. 2007; Liang et al. 2007; Virgili et al. 2009; Wanderman & Piran 2010; Howell & Coward 2013) and are possibly the result of a relativistic shock breakout (Nakar & Sari 2012).

Further considerations on the possible association between FRBs and GRBs and the other classes mentioned above are based on the relative volumetric rates. Although the FRB rate does depend on the redshift distribution, which is essentially unknown, using DM_E as a proxy for distance and assuming that the observed population is uniformly distributed within $z \lesssim 1$, a rate of $\lesssim 10^4$ Gpc^{-3} yr^{-1} is obtained (Crawford et al. 2016;

Rane et al. 2016; Scholz et al. 2016), which is not too different from the local one of Ib/c SNe (Dahlen et al. 2004; Li et al. 2011; Cappellaro et al. 2015). Our conjecture that long (i.e., not *ll*-) cosmological GRBs are not associated with the Lorimer burst is consistent with the different local volumetric rate of GRBs: $1.3^{+0.6}_{-0.7} f_b^{-1}$ Gpc^{-3} yr^{-1} (Wanderman & Piran 2010) is $\sim$10–100 times lower than that of FRBs even after accounting for a $f_b^{-1} = 100$ beaming-corrected fraction. Somewhat higher values are obtained for short GRBs, whose rate is 4–$8 f_b^{-1}$ Gpc^{-3} yr^{-1} (Coward et al. 2012; Wanderman & Piran 2015). Although poorly constrained, the BNS rate of 1540^{+3200}_{-1220} Gpc^{-3} yr^{-1} from the recent gravitational wave observations (Abbott et al. 2017b) is not too far from that of FRBs. While a *ll*-GRB associated with the Lorimer burst is not excluded, their estimated local rate ($\sim$200–300 f_b^{-1} Gpc^{-3} yr^{-1} with a lower f_b^{-1} than for long GRBs; Soderberg et al. 2006; Liang et al. 2007) is also significantly lower than that of FRBs.

5. Conclusions

Motivated by the possible and controversial detection of a transient hard X/γ-ray source positionally and temporally compatible with FRB 131104, we considered the brightest Lorimer FRB and examined the data of *BeppoSAX*/GRBM, one of the most sensitive instruments that in principle could have detected any simultaneous emission in the keV–MeV band. A previous upper limit on the γ-ray fluence of 2×10^{-7} erg cm^{-2} in the Konus/*WIND* passband was already adopted in the past (Tendulkar et al. 2016). However, this value is not the outcome of any specific data analysis, but merely corresponds to the lowest fluence detected in the Konus/*WIND* GRB catalog: this is because (i) the detection efficiency in the lowest end of the fluence distribution is likely to be significantly below 1; (ii) the typical duration of a GRB is one order of magnitude less than the transient signal possibly associated with FRB 131104; (iii) no specific analysis in that energy band at the time of the Lorimer burst has been reported yet. Based on our analysis we rule out a γ-ray counterpart for the Lorimer burst with the same radio/γ-ray fluence ratio as that of FRB 131104. Furthermore, the combination of a very high specific flux and a relatively low DM strongly suggests this FRB to be a relatively nearby FRB. We used our fluence upper limits to investigate a possible relation of FRB sources with other classes of transient phenomena. We rule out an extragalactic magnetar flare analogous to that of the Galactic source SGR 1806-20, as well as a typical long GRB. Instead, a low-luminosity GRB or a sub-energetic short GRB (such as a standard short GRB viewed off-axis, as was probably the case of GRB 170817A associated to the first binary NS merger) cannot be excluded. These results, along with the comparison of the relative volumetric rates of the corresponding populations, do not rule out the possible association of FRBs with either binary NS mergers or with *ll*-GRBs, which, however, looks incompatible with a naive one-to-one correspondence.

Appendix
Background Modeling

We conveniently split the data set into individual orbits: the data available for each orbit consist of 1 s ratemeters continuously acquired in both 40–700 and >100 keV energy bands, covering the time interval from the end of a given passage over the South Atlantic Anomaly to the beginning of the next one. Hereafter, times are referred to the FRB time. The FRB orbit, spanning from −2200 to +2770 s, is affected by no classified transient event, such as GRBs (Frontera et al. 2009), solar X-ray flares, or magnetar outbursts. We estimated the background rates for each unit and energy band using the data of the fifteenth previous orbit (hereafter, referred to as the "background orbit"), during which the spacecraft had the same attitude as for the FRB orbit. The central time of the background orbit precedes that of the FRB one by 85,505 s, i.e., only 655 s difference from a sidereal day: this way, not only do both orbits experience the same configuration with respect to the Earth magnetic field, but they also share a very similar visible portion of the sky. Data were cleaned from a few spikes due to high-energy charged particles: this was done by replacing the $>7\sigma$ excesses with respect to a moving average with statistical realizations of the local average, after verifying that the same excesses were not present in different detectors, so as to exclude an electromagnetic wave origin. We therefore interpolated the rates of the background orbit in terms of Legendre polynomials up to degree 20, upon renormalizing the time span of the orbit to the $[-1, 1]$ interval. The reason behind this choice lies in their orthogonality and easier comparison between the variance of a given time series, as described by its Legendre spectrum, and that of another series, with respect to using generic polynomials. A more detailed justification will be supplied in a future dedicated work. The quality of the interpolation was verified by applying a normality test on the residuals,[6] a χ^2 test, and a runs test[7] to ensure that no trend was present. All the corresponding p-values were above the 1% threshold.

We then subtracted the background model for each unit and energy band from the corresponding data of the FRB orbit and checked the quality of the result through the same statistics as above: the worst reduced χ^2 was 1.12, while the lowest p-value for the runs test was 5%, thus confirming the robustness of the background modeling. This procedure benefited from the low variability of the equatorial orbit of *BeppoSAX* (Frontera et al. 1997).

ORCID iDs

C. Guidorzi ◉ https://orcid.org/0000-0001-6869-0835
M. Marongiu ◉ https://orcid.org/0000-0002-5817-4009
R. Martone ◉ https://orcid.org/0000-0002-0335-319X
L. Amati ◉ https://orcid.org/0000-0001-5355-7388
F. Frontera ◉ https://orcid.org/0000-0003-2284-571X
L. Nicastro ◉ https://orcid.org/0000-0001-8534-6788
M. Orlandini ◉ https://orcid.org/0000-0003-0946-3151
R. Margutti ◉ https://orcid.org/0000-0003-4768-7586
E. Virgilli ◉ https://orcid.org/0000-0003-2279-9119

---

[6] We used the python function "normaltest," based on D'Agostino and Pearson's test, as implemented in the SCIPY.STATS package.

[7] We used the python function "wald_wolfowitz" from the SKIDMARKS package.

References

Aartsen, M. G., Ackermann, M., Adams, J., et al. 2018, ApJ, 857, 117
Abbott, B. P., Abbott, R., Abbott, T. D., et al. 2017a, ApJL, 848, L13
Abbott, B. P., Abbott, R., Abbott, T. D., et al. 2017b, PhRvL, 119, 161101
Albert, A., André, M., Anghinolfi, M., et al. 2019, MNRAS, 482, 184
Alexander, K. D., Berger, E., Fong, W., et al. 2017, ApJL, 848, L21
Alexander, K. D., Margutti, R., Blanchard, P. K., et al. 2018, ApJL, 863, L18
Amati, L., Della Valle, M., Frontera, F., et al. 2007, A&A, 463, 913
Atwood, W. B., Abdo, A. A., Ackermann, M., et al. 2009, ApJ, 697, 1071
Bannister, K. W., Deller, A. T., Phillips, C., et al. 2019, Sci, 365, 565
Barthelmy, S. D., Barbier, L. M., Cummings, J. R., et al. 2005, SSRv, 120, 143
Boella, G., Butler, R. C., Perola, G. C., et al. 1997, A&AS, 122, 299
Buccantini, N., Quataert, E., Arons, J., Metzger, B. D., & Thompson, T. A. 2007, MNRAS, 380, 1541
Caleb, M., Stappers, B. W., Rajwade, K., & Flynn, C. 2019, MNRAS, 484, 5500
Campana, S., Mangano, V., Blustin, A. J., et al. 2006, Natur, 442, 1008
Cappellaro, E., Botticella, M. T., Pignata, G., et al. 2015, A&A, 584, A62
Chatterjee, S., Law, C. J., Wharton, R. S., et al. 2017, Natur, 541, 58
CHIME/FRB Collaboration, Amiri, M., Bandura, K., et al. 2019, Natur, 566, 235
Cordes, J. M., & Wasserman, I. 2016, MNRAS, 457, 232
Coward, D. M., Howell, E. J., Piran, T., et al. 2012, MNRAS, 425, 2668
Crawford, F., Rane, A., Tran, L., et al. 2016, MNRAS, 460, 3370
Dahlen, T., Strolger, L.-G., Riess, A. G., et al. 2004, ApJ, 613, 189
DeLaunay, J. J., Fox, D. B., Murase, K., et al. 2016, ApJL, 832, L1
Eftekhari, T., & Berger, E. 2017, ApJ, 849, 162
Fan, Y.-Z., & Xu, D. 2006, MNRAS, 372, L19
Feroci, M., Hurley, K., Duncan, R. C., & Thompson, C. 2001, ApJ, 549, 1021
Fong, W., Berger, E., Margutti, R., & Zauderer, B. A. 2015, ApJ, 815, 102
Frontera, F., Costa, E., dal Fiume, D., et al. 1997, A&AS, 122, 357
Frontera, F., Guidorzi, C., Montanari, E., et al. 2009, ApJS, 180, 192
Gao, H., & Zhang, B. 2017, ApJL, 835, L21
Gehrels, N., Chincarini, G., Giommi, P., et al. 2004, ApJ, 611, 1005
Gompertz, B. P., O'Brien, P. T., Wynn, G. A., & Rowlinson, A. 2013, MNRAS, 431, 1745
Gourdji, K., Michilli, D., Spitler, L. G., et al. 2019, ApJL, 877, L19
Granot, J., Guetta, D., & Gill, R. 2017, ApJL, 850, L24
Guidorzi, C., Lacapra, M., Frontera, F., et al. 2011, A&A, 526, A49
H.E.S.S. Collaboration, Abdalla, H., Abramowski, A., et al. 2017, A&A, 597, A115
Howell, E. J., & Coward, D. M. 2013, MNRAS, 428, 167
Hurley, K., Boggs, S. E., Smith, D. M., et al. 2005, Natur, 434, 1098
Jager, R., Mels, W. A., Brinkman, A. C., et al. 1997, A&AS, 125, 557
Katz, J. I. 2014, PhRvD, 89, 103009
Katz, J. I. 2016, ApJ, 818, 19
Katz, J. I. 2018, PrPNP, 103, 1
Kisaka, S., Ioka, K., & Sakamoto, T. 2017, ApJ, 846, 142
Kocevski, D., Ryde, F., & Liang, E. 2003, ApJ, 596, 389
Kulkarni, S. R., Frail, D. A., Wieringa, M. H., et al. 1998, Natur, 395, 663
Kumar, P., & Zhang, B. 2015, PhR, 561, 1
Lazzati, D., Ramirez-Ruiz, E., & Ghisellini, G. 2001, A&A, 379, L39
Li, W., Chornock, R., Leaman, J., et al. 2011, MNRAS, 412, 1473
Liang, E., Zhang, B., Virgili, F., & Dai, Z. G. 2007, ApJ, 662, 1111
Lorimer, D. R., Bailes, M., McLaughlin, M. A., Narkevic, D. J., & Crawford, F. 2007, Sci, 318, 777
Lyutikov, M., Burzawa, L., & Popov, S. B. 2016, MNRAS, 462, 941
Macquart, J.-P., & Ekers, R. D. 2018, MNRAS, 474, 1900
MAGIC Collaboration, Acciari, V. A., Ansoldi, S., et al. 2018, MNRAS, 481, 2479
Margutti, R., Alexander, K. D., Xie, X., et al. 2018, ApJL, 856, L18
Margutti, R., Berger, E., Fong, W., et al. 2017, ApJL, 848, L20
Mazets, E. P., Golentskii, S. V., Ilinskii, V. N., Aptekar, R. L., & Guryan, I. A. 1979, Natur, 282, 587
Meegan, C., Lichti, G., Bhat, P. N., et al. 2009, ApJ, 702, 791
Metzger, B. D., Berger, E., & Margalit, B. 2017, ApJ, 841, 14
Metzger, B. D., Giannios, D., Thompson, T. A., Buccantini, N., & Quataert, E. 2011, MNRAS, 413, 2031
Metzger, B. D., Quataert, E., & Thompson, T. A. 2008, MNRAS, 385, 1455
Montanari, E., Frontera, F., Guidorzi, C., & Rapisarda, M. 2005, ApJL, 625, L17

Murase, K., Kashiyama, K., & Mészáros, P. 2016, MNRAS, 461, 1498
Murase, K., Mészáros, P., & Derek, B. 2017, ApJL, 836, L6
Nakar, E., & Sari, R. 2012, ApJ, 747, 88
Nicholl, M., Williams, P. K. G., Berger, E., et al. 2017, ApJ, 843, 84
Niino, Y. 2018, ApJ, 858, 4
Norris, J. P., & Bonnell, J. T. 2006, ApJ, 643, 266
Palaniswamy, D., Li, Y., & Zhang, B. 2018, ApJL, 854, L12
Palaniswamy, D., Wayth, R. B., Trott, C. M., et al. 2014, ApJ, 790, 63
Palmer, D. M., Barthelmy, S., Gehrels, N., et al. 2005, Natur, 434, 1107
Petroff, E., Barr, E. D., Jameson, A., et al. 2016, PASA, 33, e045
Petroff, E., Hessels, J. W. T., & Lorimer, D. R. 2019a, A&ARv, 27, 4
Petroff, E., Oostrum, L. C., Stappers, B. W., et al. 2019b, MNRAS, 482, 3109
Planck Collaboration, Ade, P. A. R., Aghanim, N., et al. 2016, A&A, 594, A13
Popov, S. B., Postnov, K. A., & Pshirkov, M. S. 2018, PhyU, 61, 965
Rane, A., & Lorimer, D. 2017, JApA, 38, 55
Rane, A., Lorimer, D. R., Bates, S. D., et al. 2016, MNRAS, 455, 2207
Ravi, V. 2019, MNRAS, 482, 1966
Ravi, V., Catha, M., D'Addario, L., et al. 2019, Natur, 572, 352
Romero, G. E., del Valle, M. V., & Vieyro, F. L. 2016, PhRvD, 93, 023001
Rowlinson, A., O'Brien, P. T., Tanvir, N. R., et al. 2010, MNRAS, 409, 531
Scholz, P., Bogdanov, S., Hessels, J. W. T., et al. 2017, ApJ, 846, 80
Scholz, P., Spitler, L. G., Hessels, J. W. T., et al. 2016, ApJ, 833, 177

Shannon, R. M., Macquart, J. P., Bannister, K. W., et al. 2018, Natur, 562, 386
Shannon, R. M., & Ravi, V. 2017, ApJL, 837, L22
Soderberg, A. M., Kulkarni, S. R., Nakar, E., et al. 2006, Natur, 442, 1014
Spitler, L. G., Scholz, P., Hessels, J. W. T., et al. 2016, Natur, 531, 202
Tendulkar, S. P., Bassa, C. G., Cordes, J. M., et al. 2017, ApJL, 834, L7
Tendulkar, S. P., Kaspi, V. M., & Patel, C. 2016, ApJ, 827, 59
Thompson, C. 1994, MNRAS, 270, 480
Thornton, D., Stappers, B., Bailes, M., et al. 2013, Sci, 341, 53
Troja, E., Lipunov, V. M., Mundell, C. G., et al. 2017, Natur, 547, 425
Tsvetkova, A., Frederiks, D., Golenetskii, S., et al. 2017, ApJ, 850, 161
Usov, V. V. 1992, Natur, 357, 472
Virgili, F. J., Liang, E.-W., & Zhang, B. 2009, MNRAS, 392, 91
Wanderman, D., & Piran, T. 2010, MNRAS, 406, 1944
Wanderman, D., & Piran, T. 2015, MNRAS, 448, 3026
Waxman, E., Mészáros, P., & Campana, S. 2007, ApJ, 667, 351
Xi, S.-Q., Tam, P.-H. T., Peng, F.-K., & Wang, X.-Y. 2017, ApJL, 842, L8
Xu, J., & Han, J. L. 2015, RAA, 15, 1629
Yamasaki, S., Totani, T., & Kawanaka, N. 2016, MNRAS, 460, 2875
Yang, Y.-H., Zhang, B.-B., & Zhang, B. 2019, ApJL, 875, L19
Zhang, B. 2018, ApJL, 867, L21
Zhang, B.-B., & Zhang, B. 2017, ApJL, 843, L13
Zhang, S.-B., Hobbs, G., Dai, S., et al. 2019, MNRAS, 484, L147